

Z-Scanning of Multiple-Pulse Laser Ablation of Copper Study for Application in Roll-Printed Electronics

Cao Xuan Binh, Vu Tien Dung, Vu Toan Thang, Nguyen Thi Kim Cuc*

Hanoi University of Science and Technology, Ha Noi, Vietnam

*Corresponding author email: cuc.nguyenthikim@hust.edu.vn

Abstract

The benefits of pulsed laser ablation in advanced manufacturing have been studied in terms of intensity, adequate orientation, damped noise, and great adaptability. During ultrashort laser ablation, the interaction between a copper surface and numerous pulses was explored to establish ideal focusing conditions. We present a simple theoretical description of morphological changes in the ablated channel and illustrate its utility in real-time placement of the interactive surface at the focus during multiple-pulse laser ablation of copper. The experimental results for copper ablation depth indicate that combining a dynamic focusing mechanism and a theoretical formula for ablation-cycle-dependent ablation depth allows one to regulate the geometry of ablated channels. This model can be applied to a wide range of high-efficiency ablation systems and could be crucial in the development of a high-precision ablation system for the curved surfaces in highly scaled copper gravures used in printed electronics, which currently presents an engineering problem.

Keywords: Roll printed electronics, multiple-pulse laser, laser ablation, optimal focusing.

1. Introduction

The interaction of an ultrashort pulsed laser with materials, as well as the physical events that result from it, has been extensively researched [1]. Due to its high intensity, appropriate alignment, damped noise, and adaptability, pulsed laser ablation has recently shown enormous benefits in modern manufacturing. This manufacturing technique has several applications, involving circuit printing and nanoparticle/nanosheet production [2]. The appearance and accuracy of the created product are determined by the ablation beam's concentrating condition on a micro-sized area on the workpiece's surface. In the created surface, an out-of-focus laser causes inhomogeneous patterns, collected debris, and local damage. To ensure uniformity and aesthetics, the ablation surface should be carefully maintained at the laser focus during processing, with the laser focus being changed to accurately follow alterations in morphology at the interactive ablation surface during the ablation process. Reflection-based, interferometry-based, and confocal focusing methods have been introduced, as well as other sophisticated optical approaches [3], proposed by H.-S. Kim *et al.* and J. Jivraj used focus stabilization to identify defects in wide optical surfaces [4], concentrating on the applications of these advanced focusing systems. However, the bulk of prior solutions make it difficult to detect the laser focus on a non-planar surface in real time; also, these systems are non-user friendly. A credible theoretical model that reflects the interaction between the material and the ablation laser, as well as the change in topography caused by the ablation laser

throughout processing, is required for a precise and flexible focusing condition.

Several researchers developed theoretical models to explain the morphological diversity in ablated patterns during pulsed-laser ablation [5]. Furthermore, H. Pazokian, C. Lei *et al.*, and K. Luo *et al.* explored alterations in ablated channel profile during laser processing [6]. T.-H. Chen *et al.* and A. Zemaitis *et al.* recently presented an ablation efficiency formula and provided ways for enhancing this parameter in ultrashort laser ablation [7]. While analytical models abound, no one has yet suggested combining a precise analytical model and an experimental design for establishing tight focusing conditions during ultrashort laser ablation.

The preservation of tight focusing conditions on the interaction surface assists in the formation of U-shaped cells on the surface of the copper gravure in roll printed electronics. In contrast to V-shaped cells, which have a rounded bottom, U-shaped cells are crucial in gravure printing (Fig. 1). The printing procedure is as follows. Microscopically tiny cells are imprinted on the surface of a cylindrical gravure. The conducting ink is delivered to the cells from an ink reservoir, and the doctor blade guarantees that the filled-in ink volume is exactly equivalent to the cell volume. Due to the sheer pressure produced by the imprint roller, the ink is thoroughly transferred to the substrate, forming a small electrical circuit.

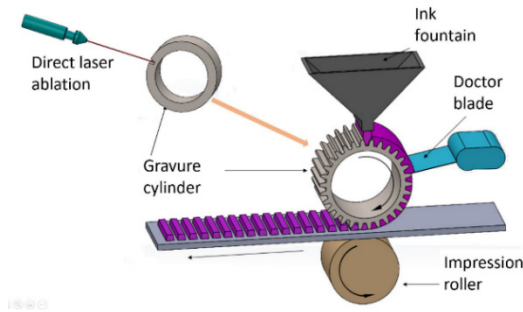


Fig. 1. Gravure printing process.

Typically, V-shaped cells are created by setting the ablation laser focus location. Meanwhile, U-shaped cells have a smaller surface area to volume ratio than V-shaped cells, resulting in a lower adhesive force between the cell and fluid; hence, U-shaped cells may be emptied more readily than V-shaped cells when the ink is transferred from the gravure cells to the substrate. Furthermore, when ink drops from U-shaped cells are transferred to the substrate, they spread and combine to create a line. The droplets merge to create a smooth continuous line in U-shaped cells; but, in V-shaped cells, when a tight focusing condition is not maintained, the drops are more likely to produce discontinuous patches or scalloped lines on the substrate [8]. As a result, real-time placement of the ablation laser focus on the target surface is critical for controlling the cell form on the roll gravure and, as a result, optimizing the filling and release of conducting ink throughout the printing process, which determines the quality of printed electronics.

This paper delivers the investigation of the interaction of a copper surface and an ultrashort laser pulse analytically to determine the dynamical change in ablation depth during laser ablation of a copper used in roll printed electronics. The theoretical model is then combined with a dynamic focusing device to keep the workpiece surface focused during the ultrashort laser ablation process. Throughout the ablation process, the laser focus follows the change of the ablation depth. This automated laser focus adjustment on an interactive surface is demonstrated to regulate the ablated hole shape and boost ablation efficiency. This advantage is critical in printed electronics, where homogenous patterns with U shapes on the printing gravure surface are required. A new generation of high-precision, high-efficiency ablation systems was established by applying the theoretical evolution of ablation depth to a dynamic focusing system, providing a versatile micromachining method for highly scaled copper gravures.

2. Methodology

The experimental process is presented as follows. First, an experimental schematic diagram of dynamic focusing system is shown as a template for applying a theoretical model of ablation depth evolution during the ablation process. Second, the interaction between

the copper sample surface and laser pulses is investigated to determine the development of ablation depth as a function of incident pulse count and ablation laser scanning cycles. Experimental findings are provided to demonstrate the suggested theoretical model's dependability and applicability. Finally, some thoughts and conclusions on the proposed approach are presented.

The ablation setup is shown in Fig. 2. A dynamic focusing system shifts the ablation laser's focal point along the z -axis to focus the ablation laser on the sample surface. The system includes three lenses: a negative lens L_1 (f_1), a positive lens L_2 (f_2), and an objective lens L_3 (f_3). Lenses L_2 and L_3 are fixed at their positions by a micro-positioning stage, L_1 is shifted around the initial position, at which the beam between L_2 and L_3 is collimated to adjust the focal position of the ablation laser along the z -axis. The following is the relation between the $L_1 - L_2$ distance h and the distance u between the laser focal position and the objective lens L_3 [9]:

$$h = -\frac{f_2^2}{f_3^2}u + \frac{f_2^2}{f_3} + f_1 + f_2 \quad (1)$$

As a result, the negative lens L_1 displacement to laser focal position displacement ratio is:

$$\frac{\Delta h}{\Delta u} = -\frac{f_2^2}{f_3^2} \quad (2)$$

In practice, the focal length of the positive f_2 should be significantly greater than that of the objective lens f_3 because the laser focus must be shifted by exceedingly small distance Δu while the positive lens should not move a distance Δh less than the micro-positioning stage limit. Furthermore, the focal spot size is found to vary only slightly, with a deviation of less than 1%; meanwhile, the lens L_1 is shifted by a few millimeters from its initial position. The sample is moved along the y -axis (Fig. 2) during the ablation process to allow a multiple-pulse laser to create the surface channel.

At the focal point, overlapping successive laser pulses create the channel. The whole cycle concludes when the channel is finished. The multiple-pulse laser's real-time z -scanning is intended to keep the laser focus on the interacting surface of the sample; hence, after each ablation cycle along the y -axis, the laser focus is changed by a distance equal to the channel depth corresponding to the shift of the negative lens L_1 along the z -axis. Thus, during ultrashort laser ablation, ideal focusing conditions are established and automatically supported. The development of the ablation depth after each ablation cycle will be computed in the next section to automatically alter the emphasis on the interactive surface.

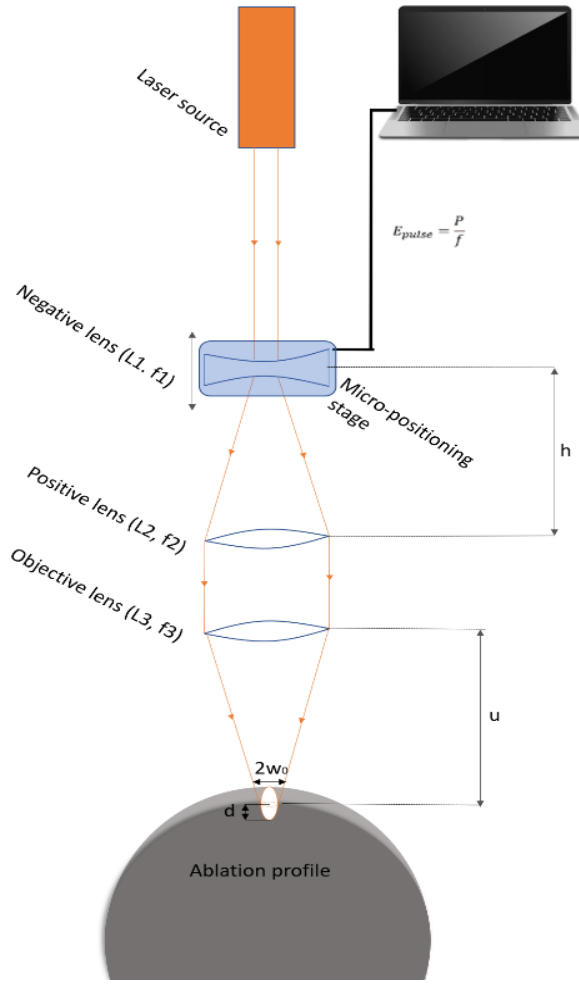


Fig. 2. Schematic diagram of real-time z -scanning for multiple-pulse laser ablation on a cylindrical groove.

3. Principal of Laser Ablation

As shown graphically in Fig. 2, the theoretical model quantifies the overall ablation process. The dynamic focusing mechanism described in the preceding section focuses the laser pulse onto the copper surface. The distance between the laser focal position and the objective lens $z_f = u$ can be tuned by shifting the negative lens L_1 . The beam spot size at the interactive surface (focal plane) can be calculated as $w(z') = w_0 \sqrt{1 + \left(\frac{z'}{z_R}\right)^2}$ where $z' = z - z_f$ is the defocus distance from the surface to the laser focus ($z_f = u$) and $z_R = \frac{\pi w_0^2}{\lambda}$ is the Rayleigh length.

The laser beam is scanned along the y -axis at v and f repetition rates, resulting in an ablated channel with a profile of $H(x)$ along the y -axis. To build a simple theoretical model for multiple-pulse laser ablation, we assume that the physical parameters of temperature, electron heat capacity, electron density, and absorption coefficient are time-independent during each pulse (τ) and that at surface temperatures comparable to the Fermi level, only free electrons

participate in heat conduction as an ideal gas ($c_e = \frac{3}{2}$) (free electron model). Furthermore, the temperature at the interaction surface is homogenous during each pulse.

3.1. Laser Penetration

Considering a laser pulse that is focused on a copper surface and penetrates the metal's interior. The laser field is exponentially diminished in this process dependent on the depth of laser penetration in the material owing to optical absorption of the laser photons [5]. The laser electric field $E(x, y, z)$ diminishes in three directions (x, y, z) as the sample penetration depth increases:

$$\nabla E = -\frac{E(z)}{3l_s} = \frac{dE(z)}{dz}$$

$$\rightarrow E(z) = E(0) \exp\left(-\frac{z}{3l_s}\right) \quad (3)$$

where z is the laser penetration depth into the material and l_s is the effective penetration length determined from $l_s = \frac{c}{\omega k}$ (k is the imaginary part of the refractive index derived from the dielectric function of the object material, and ω is the frequency of the incident laser)

3.2. Acceleration of Electrons in Metal

All laser energy collected by the copper is transformed into kinetic energy for free electrons throughout this process. The incident laser, in effect, warms the electron gas along its propagation path, as indicated by the energy conservation law in an ideal case [5]:

$$c_e n_e \frac{\partial \varepsilon_e}{\partial t} = -\frac{dQ}{dz} \quad (4)$$

where $n_e = \frac{8\sqrt{2}\pi m^{\frac{3}{2}}}{h^3} \left(\frac{2}{3} \varepsilon_F^{\frac{3}{2}}\right)$ is the electron density of the copper and I_o is the incident laser intensity. The thermal energy is transferred from the absorbed laser energy, which is proportional to the laser intensity ($I(z) \sim E(z)^2$) and the temperature-dependent absorption coefficient $a = 1 - r = \frac{4n}{(n+1)^2 + k^2}$, in which n and k are the refractive index and extinction coefficient:

$$Q = a I_o \exp\left(-\frac{2z}{3l_s}\right) \quad (5)$$

The electron energy in (3) is calculated as:

$$\varepsilon_e(z) = \frac{4a I_o t}{9n_e l_s} \exp\left(-\frac{2z}{3l_s}\right) \quad (6)$$

3.3. Ablation Threshold

The sum of the electron work function ε_w and the atomic binding energy or heat of evaporation of the copper ε_b is defined as the total energy for ablation

during a single pulse τ . During a single pulse, this energy is barely sufficient to eject electrons and ions from the copper surface ($z = 0$):

$$\varepsilon_e(0) = \varepsilon_b + \varepsilon_w = \frac{4aI_o\tau}{9n_e l_s} \quad (7)$$

The incident intensity required to eject electrons and ions from the copper surface is given by the quantity I_o for a single pulse. The fluence at the ablation threshold is then figured out:

$$F_{th} = aI_o\tau = \frac{9n_e l_s(\varepsilon_b + \varepsilon_w)}{4} \quad (8)$$

To validate this model, the ablation threshold fluences of copper were estimated when ablated by lasers with wavelengths of 780 nm and 1053 nm, respectively, and compared to earlier study results. The parameters for copper are $n_e = 8.45 \times 10^{28}$, $\varepsilon_b = 3.125$ eV, $\varepsilon_w = 4.65$ eV, and $\lambda = 780$ nm. The ablation threshold fluence is calculated as $(F_{th})_{Cu} = 0.61$ J/cm², which is consistent with the data shown in the experimental figure in [10], where the copper plate is ablated at approximately $F = 0.6$ J/cm².

3.4. Heat Accumulation Model

The ablation threshold for a static laser source reduces with each pulse, according to the heat buildup principle [11]. As more laser pulses N come, the threshold drops, allowing the surface to be ablated more easily:

$$F_{th}(N, w(z')) = \frac{9n_e l_s(\varepsilon_b + \varepsilon_w)}{4} \times \left(\frac{\frac{8\delta}{w(z')^2 f}}{\ln\left(1 + \frac{8\delta}{w(z')^2 f}(N-1)\right)} \right) \quad (9)$$

where δ is the thermal diffusivity of the copper and f is the laser repetition rate. The depth of the ablated hole after the first pulse depends on the incident laser pulse energy and the threshold fluence based on the Beer-Lambert model:

$$d(N = 1) = \frac{3}{2} l_s \ln\left(\frac{F}{F_{th}(1, w(z'))}\right) \quad (10)$$

The absorbed flux of a moving incident laser with speed v and pulse duration τ is calculated as follows [6]:

$$\begin{aligned} F(P, w(z'), x) &= \frac{2P}{\pi w^2(z')} a \int_0^\infty dt e^{-\frac{2(x^2+y^2)}{w^2(z')}} e^{-4\frac{t^2}{\tau^2} \ln 2} \\ &= \frac{P}{\pi w^2(z')} a \sqrt{\frac{\pi}{2\left(\frac{v^2}{w^2(z')} + \frac{2\ln 2}{\tau^2}\right)}} e^{-\frac{2x^2}{w^2(z')}} \end{aligned} \quad (11)$$

where P is the laser power and r is the radial coordinate in the xy -plane. Therefore, the beam profile has a paraboloid form, as follows:

$$\begin{aligned} z(N = 1) &= \frac{3}{2} l_s \ln\left(\frac{F(P, w(z'), x)}{F_{th}(1, w(z'))}\right) = \frac{3}{2} l_s \times \\ &\ln\left(\frac{P}{\pi w^2(z') F_{th}(1, w(z'))} a \times \sqrt{\frac{\pi}{2\left(\frac{v^2}{w^2(z')} + \frac{2\ln 2}{\tau^2}\right)}}\right) - \frac{3l_s x^2}{w^2(z')} \end{aligned} \quad (12)$$

The ablation depth after the first pulse is calculated when $x = 0$:

$$\begin{aligned} d(N = 1) &= \frac{3}{2} l_s \times \\ &\ln\left(\frac{P}{\pi w^2(z') F_{th}(1, w(z'))} a \times \sqrt{\frac{\pi}{2\left(\frac{v^2}{w^2(z')} + \frac{2\ln 2}{\tau^2}\right)}}\right) \end{aligned} \quad (13)$$

The laser beam moves with velocity v and repetition rate f along the y -axis, and the number of pulses needed to cover a beam spot area along the scanning channel during the first ablation cycle is:

$$N = \frac{2w(z')f}{v} \quad (14)$$

The laser focus is positioned on the copper surface with $w(z') = w_o$, and the depth of the laser-ablated holes after the first cycle is defined when $x = 0$:

$$\begin{aligned} d(1st) &= \frac{3}{2} l_s \sum_{n=1}^{N=\frac{2w_o f}{v}} S_{pulse} \times \ln\left(\frac{F(P, w_o, 0)}{F_{th}(n, w_o)}\right) \\ &= \frac{3}{2} l_s \sum_{n=1}^{N=\frac{2w_o f}{v}} \frac{2w_o - \frac{(n-1)v}{f}}{2w_o} \times \\ &\ln\left(\frac{F(P, w_o, 0)}{F_{th}(n, w_o)}\right) \end{aligned} \quad (15)$$

where S_{pulse} is the overlap of each pulse over the beam spot area [12]. After the first cycle, the laser is scanned again on the same channel to increase the depth. At this point, if the focus is fixed, the beam spot size at the interactive surface is $w(z') = w(d(1st))$. The total depth after the second cycle is:

$$\begin{aligned} d(2nd) &= \frac{3}{2} l_s \sum_{n=1}^{N=\frac{2w_o f}{v}} \frac{2w_o - \frac{(n-1)v}{f}}{2w_o} \times \ln\left(\frac{F(P, w_o, 0)}{F_{th}(n, w_o)}\right) + \\ &\frac{3}{2} l_s \times \sum_{n=1}^{N=\frac{2w(d(1st))f}{v}} \frac{2w(d(1st)) - \frac{(n-1)v}{f}}{2w(d(1st))} \times \\ &\ln\left(\frac{F(P, w(d(1st)), 0)}{F_{th}(n, w(d(1st)))}\right) \end{aligned} \quad (16)$$

The total depth after the N th cycle is as presented in [14] follows:

$$d(Nth) = A_1 + A_2 + A_3 + \dots + A_n \quad (17)$$

where:

$$A_1 = \frac{3}{2} l_s \sum_{n=1}^{N=\frac{2w_o f}{v}} \frac{2w_o - \frac{(n-1)v}{f}}{2w_o} \times \ln \left(\frac{F(P, w_o, 0)}{F_{th}(n, w_o)} \right)$$

$$A_2 = \frac{3}{2} l_s \sum_{n=1}^{N=\frac{2w(d(1st))f}{v}} \frac{2w(d(1st)) - \frac{(n-1)v}{f}}{2w(d(1st))} \times \ln \left(\frac{F(P, w(d(1st)), 0)}{F_{th}(n, w(d(1st)))} \right)$$

$$A_3 = \frac{3}{2} l_s \sum_{n=1}^{N=\frac{2w(d(2nd))f}{v}} \frac{2w(d(2nd)) - \frac{(n-1)v}{f}}{2w(d(2nd))} \times \ln \left(\frac{F(P, w(d(2nd)), 0)}{F_{th}(n, w(d(2nd)))} \right)$$

$$A_n = \frac{3}{2} l_s \sum_{n=1}^{N=\frac{2w(d(N-1th))f}{v}} \frac{2w(d(N-1th)) - \frac{(n-1)v}{f}}{2w(d(N-1th))} \times \ln \left(\frac{F(P, w(d(N-1th)), 0)}{F_{th}(n, w(d(N-1th)))} \right)$$

Since the change in depth (a few microns) is far smaller than the focal depth ($z_R \approx 40 \text{ m}$), the beam spot size at the interactive surface stays constant over several dozen cycles ($w_o = w(d(1st)) = w(d(2nd)) = \dots = w(d(N-1th))$). As a result, the depth of ablation will rise linearly with the number of cycles. This linear relationship is demonstrated in the following section by performing a laser ablation experiment on copper.

4. Experimental Results and Discussion

To show the applicability of the suggested analytical model, a laser ablation experiment on copper was performed. A Trumpf laser 5050 power has been used in the experiment. The channels were created with constant laser powers of $P = 0.4, 0.8,$ and 2 W with a repetition rate of $f = 400 \text{ kHz}$, a wavelength of $\lambda = 515 \text{ nm}$, and a pulse duration of $\tau = 7 \text{ ps}$. The scanning speed of the laser on the sample surface was $v = 1000 \text{ mm/s}, 800 \text{ mm/s},$ or 400 mm/s , and the focal spot diameter was $2w_o = 3 \mu\text{m}$. To ensure the accuracy of the proposed analytical model, the focus was kept on the sample surface plane during the ablation process, and the evolution of the ablation depth after each scanning cycle was recorded using optical microscopy. Using (17), we figured out the ablation depth after a certain number of scanning cycles. Table 1 displays the copper characteristics that

were investigated at room temperature. The ablation threshold fluences of copper for the initial pulse is $(F_{th})_{Cu} = 0.61 \text{ J/cm}^2$.

Table 1. Parameters for the test.

Parameter	Cu
Work function ε_w (eV)	4.65
Binding energy ε_b (eV)	3.125
Electron density n_e (m^{-3})	8.45×10^{28}
Effective penetration length l_s for a wavelength of 515 nm (m)	1.69×10^{-8}
Thermal diffusivity δ (m^2/s)	0.1148

Fig. 3 shows the experimentally observed ablation depth as a function of scanning cycle number, while Fig. 4 demonstrates the effect of ablation cycle number on microgroove shape for different laser powers (0.4, and 0.8W). This data proves the validity and applicability of the proposed analytical model. The ablation depth increases linearly with the number of incident ablation cycles as cycle numbers and laser intensities increase, and the microgroove surfaces become smoother and more uniform. Since the absorption coefficient a and reflectivity r are temperature-dependent parameters, the ablation threshold fluence for a given copper is as well [15,16]. The parameters of ablation threshold fluence $F_{th}(N, w(z'))$, absorbed flux of the moving incident laser $F(P, w(z'), x)$, and effective penetration depth l_s in (17) cannot be explicitly calculated from the experimental conditions because the temperature of the interactive surface changes continuously during ablation at different rates, based on the scanning speed v , laser power P , wavelength λ , repetition rate f , pulse duration τ , focal spot size $2w_o$, and copper type. However, the experimental results show that the ablation depth increases linearly with the number of cycles; thus, using known parameters for specific initial ablation conditions, one can fit the theoretical formula with the experimentally acquired data to achieve a robust formula of ablation-cycle-dependent depth. From this formula, the ablation cycle dependence of ablation depth applied in the specific fitting equations shown in Fig. 3 for copper and a set of ablation conditions $(v, P, \lambda, f, \tau, w_o)$. By applying the proposed formulas (15), (16), and (17) to the micro-positioning stage with all known parameters, one can automate the movement of the negative lens L_3 during the ablation process to support the ablation laser focus on the interactive surface of a highly scaled gravure for any initial ablation conditions.

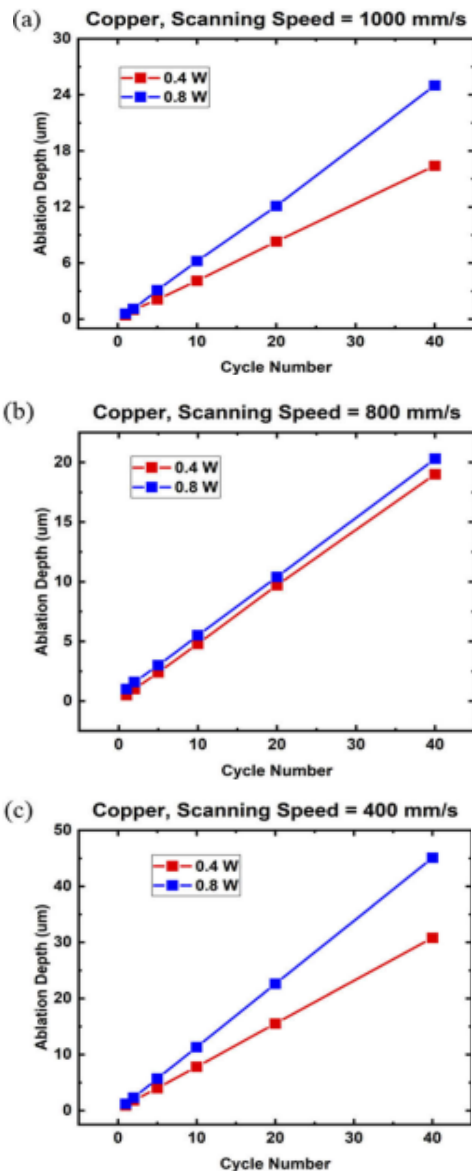


Fig. 3. Laser ablation of copper at a repetition rate of $f = 400$ kHz, a wavelength of $\lambda = 515$ nm, a pulse duration of $\tau = 7$ ps, and a focal spot diameter of $2w_0 = 3 \mu\text{m}$. (a) Scanning speed 1000 mm/s, (b) Scanning speed 800 mm/s, (c) Scanning speed 400mm/s

The flatness of the microgroove surface rises as the number of ablation cycles increases (see Fig. 4). The adhesive force between the conducting ink and the microgroove surface is lowered due to the flatness. The depth and flatness of the ablated holes may be adjusted with this approach, allowing you to tailor the aspect ratio (depth-diameter ratio) for optimal conducting ink filling and release. As a result, the conducting ink may completely fill the ablated holes on the printing gravure and be completely transferred to the substrate to form electronic structures during the gravure printing process [8].

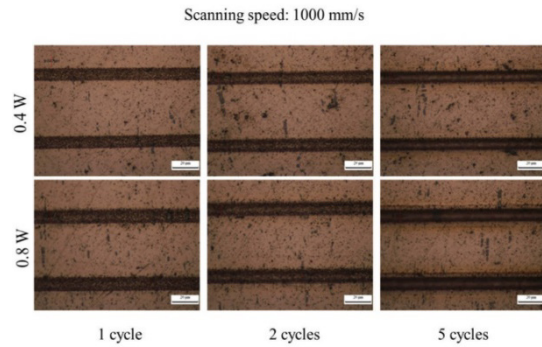


Fig. 4. Optical microscope images of microgrooves on a copper sample after 1, 2, or 5 ablation cycles at an incident power of 0.4 and 0.8 W and a scanning speed of 1000 mm/s.

5. Conclusion

In this work, a theoretical model of the interaction between a copper surface and ultrashort laser pulses was offered, as well as a strategy for controlling the shape of ablated holes during cycle-based laser ablation by maintaining tight focusing conditions for the interactive surface. To validate the derived theoretical formula, experimental laser processing was done on a copper surface. For roll electronic printing, the proposed technology has a lot of advantages. The shape and size of the electronic structure on the substrate can be controlled with varied manipulation of the ablated cell morphology on a copper gravure; hence, the function, homogeneity, and aesthetics of microelectronic circuits can be improved. Automated control of the manufacturing laser focus accomplished using the suggested formula can result in cost savings and improved precision in ultrashort laser processing, which has significant implications for ultrashort laser research and technology.

Acknowledgments

This research is funded by Vietnam National Foundation for Science and Technology Development (NAFOSTED) under grant number 103.03-2020.48.

References

- [1]. D. Zhang *et al*, Underwater persistent bubble-assisted femtosecond laser ablation for hierarchical micro/nano structuring, *Int. J. Extrem. Manuf.* 2 (2020) 015001. <https://doi.org/10.1088/2631-7990/ab729f>
- [2]. S. Loganathan, S. Santhanakrishnan, R. Bathe, and M. Arunachalam, Prediction of femtosecond laser ablation profile on human teeth, *Lasers Med. Sci.*, vol. 34, no. 4, pp. 693-701, Jun. 2019, <https://doi.org/10.1007/s10103-018-2644-0>
- [3]. B. X. Cao, P. Le Hoang, S. Ahn, J. Kim, H. Kang, and J. Noh, Real-time laser focusing system for high-precision micromachining using diffractive beam sampler and advanced image sensor, *Opt. Lasers Eng.*, vol. 107, pp. 13-20, Aug. 2018. <https://doi.org/10.1016/j.optlaseng.2018.03.002>

- [4]. Kim, H.-S., Lee, D.-H., Hyun, S., Je, S.K., Park, J. G., Bae, J. Y., Kim, G. H., Kim, I. J., Development of a reflective 193-nm DUV microscope system for defect inspection of large optical surfaces, *Appl. Sci.* 9 (2019) 5205.
<https://doi.org/10.3390/app9235205>
- [5]. E. G. Gamaly, A. V. Rode, B. Luther-Davies, Ablation of solids by femtosecond lasers: Ablation mechanism and ablation thresholds for metals and dielectrics, *Physics of Plasmas* 9 (3) (2002).
<https://doi.org/10.1063/1.1447555>
- [6]. Hedieh Pazokian, Theoretical and experimental investigations of the influence of overlap between the laser beam tracks on channel profile and morphology in pulsed laser machining of polymers, *Optik* 171 (2018) 431-436.
<https://doi.org/10.1016/j.ijleo.2018.06.066>
- [7]. T.-H. Chen, R. Fardel, and C. B. Arnold, Ultrafast z-scanning for high-efficiency laser micro-machining, *Light Sci. Appl.*, 7(4) (2018) 17181-17181.
<https://doi.org/10.1038/lsa.2017.181>
- [8]. G Grau *et al.*, Gravure-printed electronics: recent progress in tooling development, understanding of printing physics, and realization of printed devices, *Flex. Print. Electron* 1 (2016) 023002.
- [9]. B. X. Cao, P.H Le, S. Ahn, H. Kang, J. Kim, and J. Noh, Automatic real-time focus control system for laser processing using dynamic focusing optical system, *Opt. Express* 25, (2017) 28427-28441.
<https://doi.org/10.1364/OE.25.028427>
- [10]. C. Momma, S. Nolte, B. N. Chichkov, F. V. Alvensleben, A. Tunnermann, Precise laser ablation with ultrashort pulses, *Appl. Surf. Sci.* 109/110, 15 (1997).
- [11]. B. C. Stuart, M. D. Feit, S. Herman, A. M. Rubenchik, B. W. Shore, M. D. Perry, Optical ablation by high-power short-pulse lasers, *J. Opt. Soc. Am. B* 13 (1996), 459-468.
- [12]. A. Naghilou, O. Armbruster, M. Kitzler, W. Kautek, Merging spot size and pulse number dependence of femtosecond laser ablation thresholds: modeling and demonstration with high impact polystyrene, *J. Phys. Chem. C*, vol. 119(40) (2015) 22992-22998.
<https://doi.org/10.1021/acs.jpcc.5b07109>
- [13]. N. B. Dahotre *et al.*, Wetting behaviour of laser synthetic surface microtextures on Ti-6Al-4V for bioapplication, *Phil. Trans. R. Soc. A* 368 (2010) 1863-1889.
- [14]. Le Phuong Hoang, Phuong Thao Nguyen, Thi Kim Cuc Nguyen, Toan Thang Vu, and Xuan Binh Cao, Study on real-time z-scanning of multiple-pulse laser ablation of metal applied in roll-printed electronics, *Opt. Mater. Express* 11, 509-523 (2021)
- [15]. A. Abdelmalek, Z. Bedrane, E. H. Amara, B. Sotillo, V. Bharadwaj, R. Ramponi, S. Eaton, Ablation of copper films by femtosecond laser multipulse irradiation, *Appl. Sci.* 8(10) (2018) 1826.
<https://doi.org/10.1098/rsta.2010.0003>
- [16]. Yiwei Dong, Zongpu Wu, Yancheng You, Chunping Yin, Wenhui Qu, and Xiaoji Li, Numerical simulation of multi-pulsed femtosecond laser ablation: effect of a moving laser focus, *Opt. Mater. Express* 9 (2019) 4194-4208.
<https://doi.org/10.1364/OME.9.004194>